Direct Observation and Modeling of Transient Nucleation in Isothermal Thickening of Polymer Lamellar Crystal Monolayers

Yi-Xin Liu,[†] Jian-Feng Li,[‡] Dun-Shen Zhu,[†] Er-Qiang Chen,*[,†] and Hong-Dong Zhang*[,‡]

Beijing National Laboratory for Molecular Sciences, Department of Polymer Science and Engineering and Key Laboratory of Polymer Chemistry and Physics of Ministry of Education, College of Chemistry, Peking University, Beijing 100871, China, and Key Laboratory of Molecular Engineering of Polymer of Ministry of Education, Department of Macromolecular Science, Fudan University, Shanghai 200433, China

Received December 17, 2008
Revised Manuscript Received March 13, 2009

The structure and morphology stability are extremely important to the usage of crystalline polymeric materials. It is known that during polymer crystallization the chain molecules may face multiple free energy barriers (and thus with more than one minimum) in a free energy landscape. In general, as the free energy reduction follows the maximum rate path, chain molecules tempt to overcome the lowest barrier to enter a state of folded chain lamellar crystals with a thickness (fold length) around 5−50 nm, which is usually metastable.[1] Therefore, from a thermodynamic point of view, there is always a tendency for the thinner lamellae to relax into more stable state, i.e., thicker lamellae with a larger fold length. Since such a morphology evolution can greatly impact the physical properties of polymeric materials, lamellar thickening has been widely studied both experimentally and theoretically, not only with regard to fundamental issues but also for applications. However, the exact molecular mechanism of lamellar thickening, a typical topic of the metastability of condensed matter, remains ambiguous so far.

In experiments, lamellar thickening has been observed shortly after the discovery of folded chain crystals,[2] mainly based on the small-angle X-ray scattering (SAXS) measurements. The SAXS clearly revealed that the long period of lamellae increased after the formation of initial lamellar stacks. Two major features of lamellar thickening are (1) the long period increases linearly with logarithm of time (t), particularly when t is not very long, and (2) the thickening rate of long period increases along temperature (T). The lamellar thickening must result from the longitudinal diffusion of chain segments with high mobility in the crystal lattice.[3] Sanchez et al. have reproduced the experimental results by a phenomenological law, which states that the lamellar thickening is a thermodynamically irreversible process driven by a driving force arising from the unequal free energies between the fold and lateral surfaces and the nonequilibrium kinetically determined ratio of their areas.[4] However, the coherent thickening domain, as a key assumption of this theory, is physically unclear and thus cannot be confirmed by experiments. On the other hand, the observations might be interpreted to be indicative of nucleation control.[5−7] It was imagined that a bundle-like nucleus of thickened domain could form after an incubation period of chain unfolding, which would then initiate growth. Despite numerous evidence collected,[8] there is still a lack of the observations directly related to the early stage of lamellar thickening, mainly due to the limitation of techniques applied. For example, it is hard to use the scattering profiles measured from lamellar stacks to answer how a lamella starts to thicken and how lateral dimensions of a thickened domain evolve with time. In this context, whether the lamellar thickening is nucleation controlled or simply an irreversible phenomenon cannot be justified.

Recently, the real space technique of atomic force microscopy (AFM) enables the direct observation of polymer crystals down to the nanometer scale.[9,10] While the isothermal crystallization of polymers was followed in situ,[9,11,12] the lamellar thickening was investigated.[9,13−15] In this Communication, we present a detailed study on kinetics of lamellar thickening of isolated polymer crystal monolayers on solid substrates annealed at elevated Ts. In contrast to a usual polymer crystallization that occurs at three dimensions (3D), our monolayer system provides a quasi-two-dimensional (2D) example which can be explored by AFM in great detail. The monolayer feature also simplifies the theoretical consideration, allowing an effective phase field simulation. Our results manifest that monolayer lamellar thickening process follows a mechanism of nucleation and growth (NG). The birth and evolution of transient nuclei were captured with high spatial and adequate time resolution for the first time. The experimentally visualized patterns can help to understand more the general primary nucleation process. Moreover, the thickening rate increasing with T is found to be naturally associated with the decrease of fold surface energy, an important component of the thickening barrier.

The sample used in this study is a low molecular weight (LMW) poly(ethylene oxide) (PEO) fraction with both chain ends of −OH purchased from Polymer Laboratories (M_n = 2000 g mol^{-1}, M_w/M_n = 1.03). A remarkable feature of LMW PEO fraction is that it can crystallize into integral-folding chain (IF) crystals[6,16] as stacked lamellae in bulk and also as monolayers on solid surfaces with the chain axis normal to the substrate.[14] The extended chain crystal [IF(0)] of LMW PEO corresponds to the ultimate stable state, whereas other IF crystals stay at local free energy minimums. For our sample, the IF(0) thickness is almost identical to the calculated extended chain length of l_0a = 12.5 nm, where l_0 = 45 is the degree of polymerization and a = 0.2783 nm,[17] the average length of a monomer in the crystal lattice; the thickness of once-folded chain crystal [IF(1)] is simply 12.5/2 = 6.3 nm. These two discrete thicknesses can be unambiguously distinguished through AFM height measurement. The T_m of IF(0) monolayers is 51.0 °C; the T_m of IF(1) monolayers is slightly above 30.0 °C, which is unable to be precisely determined due to the fast thickening when T approaches to the T_m of IF(1).

We prepared the PEO monolayer on freshly cleaved mica surfaces by the simple static solution casting.[12] The concentration of the PEO/methylene chloride solution was ∼0.5 mg mL^{-1}, and the as-cast samples were dried in vacuum for days. To obtain the initial IF(1) monolayers, the samples were heated to 70 °C for 5 min to ensure the complete melting, followed by quenching to 18 °C or below. Isothermal thickening from IF(1) to IF(0) of the samples was realized by annealing the IF(1) monolayers at elevated Ts. The subsequent morphological changes were monitored with a tapping mode AFM (DI Nanoscope IIIA coupled with a hot stage). The AFM tip dilation

* Corresponding authors. E-mail: eqchen@pku.edu.cn (E.-Q.C.); zhanghongdong@gmail.com (H.-D.Z.).
[†] Peking University.
[‡] Fudan University.

10.1021/ma802806q CCC: $40.75
Published on Web 03/26/2009

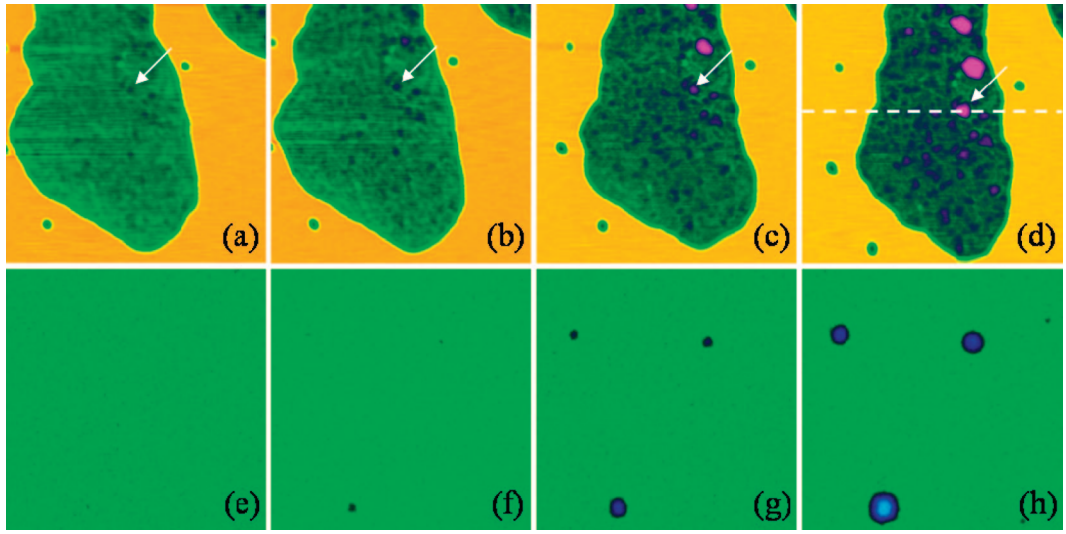

Figure 1. A set of height images (size of 800 × 800 nm^2) captured by tapping mode AFM for the thickening of a PEO monolayer crystal annealed at 26 °C (a−d) and a set of height images obtained from simulation at $T = 302.5$ K (e−h). For AFM images, the annealing time is (a) 7.0, (b) 20.2, (c) 35.9, and (d) 50.8 min; the green region is monolayer crystal, and the orange region is substrate. For simulation, the run time is (e) 300, (f) 370, (g) 440, and (h) 510 steps.

effect was examined by deconvoluting the section profiles from an assumed tip geometry function of parabola using a published surface reconstruction algorithm.[18] Because the maximum height difference between the thickened domain and the top surface of the IF(1) monolayer is only ∼6 nm, the tip dilation effect is almost negligible (see Figure S2 in the Supporting Information). Therefore, the height and lateral dimension given below were directly measured from the original AFM section profiles.

In the AFM experiments, both the topography and thickness distribution across the top surface of crystal monolayers could be visualized simultaneously. The initial IF(1) monolayers were fingerlike, similar to those crystallized from polymer thin films at a large undercooling with a diffusion-limited mechanism of crystal growth.[14] The top surface of initial IF(1) monolayer was quite smooth with a root-mean-square average height deviation (R_q) of ∼0.15 nm. However, it became rough once the temperature jumped to higher, indicating the enhanced fluctuation of lamellar thickness of the monolayer. This reflects that the increased thermal energy certainly causes the stronger chain motion along the longitudinal direction within the mother phase of IF(1) monolayer. The fluctuation eventually led to the formation of thickening domains which could be clearly identified within the mother phase in AFM height images.

Figure 1a−d shows a set of AFM height images recorded at $T = 26$ °C (as another example, a set of images for 30 °C is given in the Supporting Information). Here we focus on one branch of a fingerlike monolayer. The thickening domains recognized as the blue or purple dots in the green matrix are nearly rounded. If draw a line through the center along the fast scan direction (*X* direction) and plot the section profile for each image recorded sequentially, we can obtain the interface evolution with *t*, exemplified in Figure 2 for the domain indexed by arrow in Figure 1a−d. Two quantities are necessary to describe the evolution of such domains: the maximum thickness and the lateral size, represented by the peak value (*H*) and peak half-width (*HW*) in the interface profile (see the inset of Figure 2). At the very beginning, no clear-cut interface between thickened domains and mother phase can be identified; both *H* and *HW* are randomly distributed around their minimum values, with a fluctuation amplitude of ∼0.7 nm and a fluctuation scale of ∼15 nm. After an induction period of ∼20 min, a distinguishable thickened domain emerges: the *HW* increases linearly and *H* grows first slowly followed by a rapid approach to the thickness of IF(0) crystal. Remarkably, the sigmoidal increase of *H* resembles the long period evolution pattern observed by scattering method,[4,7] but here only a single domain is measured. This observation leads to the conclusion that lamellar thickening indeed involves a primary nucleation process.[5−7] The AFM experiments by Reiter et al. demonstrate that the thickening was mainly initiated at lamellar edges where chains experience fewer constraints and thus are more mobile.[14] However, we find that the thickening domains also frequently emerge from the monolayer interior, a phenomenon that was rarely reported. We consider that the NG mechanism should be applicable for both cases. It should be noticed that the area of the crystal monolayer shown in Figure 1a−d shrank continuously, implying that the materials transported quickly from unthickened part to thickening domains due to mass conversation.

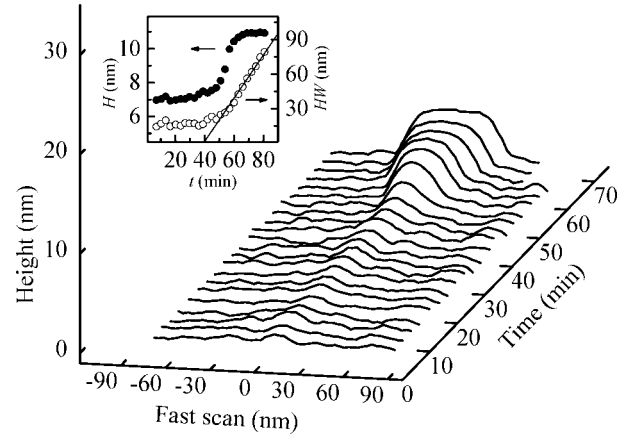

Figure 2. Section profiles through the center of a typical domain indicated by the arrow in Figure 1a−d. The inset plots the values of the peak value (*H*) and the peak half-width (*HW*) in the interface profile as functions of *t*.

The nucleation process is strongly *T*-dependent. To obtain the nucleation rate, IF(1) monolayers were annealed at various *T*s ($T \leq 30$ °C), and the number density of thickening domains (ρ_N) was counted for each images. Figure 3a illustrates a steady linear growth of ρ_N preceded by an induction period. Upon

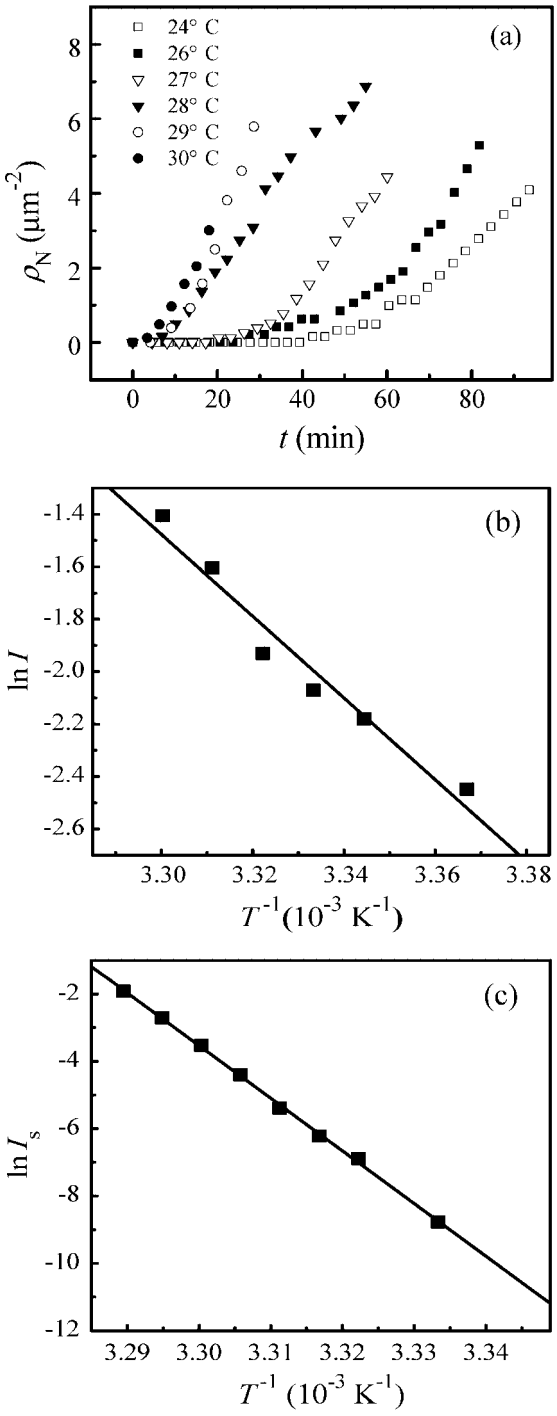

Figure 3. Evolution of the number density of thickening domains for monolayer crystals (ρ_N) annealed at various Ts (a). T-dependences of nucleation rates measured as the speed of the steady growth stage of ρ_N (b) and counted from simulation (c).

raising T, the induction period is shortened sharply and the nucleation rate is enhanced, resembling that found in bulk state. In contrast to polymer crystallization or melting where the logarithm of nucleation rate is proportional to ΔT^{-2} (ΔT is the undercooling or superheating),[8] the nucleation rate of the IF(1)-to-IF(0) transformation studied here obeys the Arrhenius law (see Figure 3b) with an activation energy of 129.7 kJ mol^{-1}.

To better understand this lamellar thickening process, we intend to build a model with consideration of the curved interface between thickening domains and mother phase. Phase field theory is widely used to study the phase transition kinetics in mesoscale.[19] This theory is often treated as a coarse-grained model by using a Landau-type free energy functional.[20] The rationale for developing such a model is the current inability of fully molecular models to address the formation of large- or mesoscale morphologies. Although this field-theoretic approach disregards most of the molecular scale details of phase transition, it is still sufficient to catch the essence of physical processes. Taking advantage of the simplicity of our 2D crystalline system, we are able to construct a free energy functional containing the well-defined physical parameters only. In our model, each stem is coarse-grained into a single point on plane associated with an order parameter ϕ defined by l/l_0, where l is the length of the stem (in monomer number) equivalent to the monolayer thickness at this lattice site. The order parameter may vary due to a cooperative sliding motion of stems along the chain axis in the crystal lattice.

It is convenient to divide the energy into two parts: local and nonlocal. The local part corresponds to the sum over the whole monolayer based on the free energy density of each stem. For a crystallized stem with length l, its free energy of crystallization in a approximation is $l(-\Delta g) = -l\Delta h_f \Delta T(T/T^0_m)$,[21] where Δg and Δh_f are the Gibbs free energy and heat of fusion per monomer, respectively, and ΔT is defined as $1 - T/T^0_m$ with T^0_m the equilibrium T_m. For convenience, we shift the zero free energy reference from melt to the IF(0) crystal so that the free energy of a stem is $f_c = l_0(1 - \phi)\Delta g$. Besides, consider a crystal monolayer with a homogeneous l and $1/2 < \phi < 1$ (i.e., the chains are nonintegrally folded); the end groups are forced to embed in the crystalline core as defects, and the folds stay on either top or bottom surface. The excess energies arisen from the defect and fold for each stem can be calculated by $f_\xi = P_\xi \xi$ and $f_\eta = P_\eta \eta$, respectively, with $\xi = 2\Delta g$ for a defect, $\eta = N_f \Delta g$ for a fold with the monomer number of N_f, and P_ξ and P_η are the l-dependent probabilities to have a defect and a fold on one stem (see Supporting Information). An additional effect related to the perturbation of stem length should also be included. Because of the inevitable thermal fluctuation,[3] a stem can adjust its length near a value corresponding to a local free energy minimum. The stem will feel a force generated by deforming the fold when it extends or contracts. Assuming the chain fold can be described by the Zachmann model,[22] this force contributes a free energy $V = 3l_0^2 k_B T(\phi - \phi')^2/2(N_f - 1)$. To sum all up, we need to minimize the free energy with respect to ϕ'. The local free energy density is

$$f_{local}(\phi) = \min_{\phi'}[f_c(\phi') + f_\eta(\phi') + f_\xi(\phi') + V(\phi, \phi')], \quad (1)$$

and the free energy of monolayer is $F_{local} = \oint_S f_{local}(\phi)\, dS$. The profile of f_{local} exhibits a double-well structure with one of IF(1) and the other of IF(0) (see Figure S4 in Supporting Information). In addition, many shallow wells are presented corresponding to other fractionally folded crystals, and the profile is in fact consisted of many upward parabolas (concave up).

The nonlocal free energy includes the surface energy of top and bottom surfaces of a crystal monolayer, while the lateral surface is neglected for a simplification.[8] Generally, the top surface is rough and its area can be expressed as an integral, while the bottom one may remain largely flat due to the incompressibility of the solid substrate. Assuming that the surface energy is independent of the surface curvature, the total surface energy can be readily calculated as

$$F_{grad} = \oint_S [\sigma_e \sqrt{1 + (\nabla z)^2} + \sigma_m]\, dx\, dy, \quad (2)$$

where σ_e and σ_m represent the top and bottom surface energies, and ∇ is the gradient operator. Further simplification is based on the assumption that the fluctuation is small enough, allowing the drop-off of the higher order spatial dependences. Using $u = x/a_0$, $v = y/a_0$ (a_0 is the square root of cross-section area of a stem), $b_\sigma = (l_0 a)^2 \sigma_e$, and $\nabla z = (l_0 a/a_0)\nabla\phi$, eq 2 is reduced to

$$F_{grad} = \oint_S \frac{b_\sigma}{2} \nabla^2\phi \, du \, dv + \oint_S (\sigma_e + \sigma_m) \, du \, dv \qquad (3)$$

The free energy functional is a combination of the local and nonlocal terms: $F(\phi) = F_{local}(\phi) + F_{grad}(\phi)$. Although the perimeter of a real initial IF(1) monolayer is always ill-shaped, we did simulation on square lattice for convenience. Because the whole area of monolayer is not conserved, we have to locate a square lattice (area S) inside the crystal monolayer (area S_0) to keep area S constant. The order parameter is nonconserved within the square lattice, but it is conserved in whole crystal monolayer with an assumption of incompressibility or mass conservation. The time evolution of nonconserved order parameter is governed by the following relaxational dynamics equation but with a correction due to incompressibility or mass conservation

$$\frac{\partial\phi}{\partial t} = -D\frac{\delta[\lambda(\phi)F(\phi)]}{\delta\phi} + \xi(\mathbf{r}, t), \qquad (4)$$

where a Lagrange multiplier $\lambda(\phi) = (S_0/S)\oint\phi_0(\mathbf{r},T) \, dS/\oint\phi(\mathbf{r},T) \, dS$ is introduced to ensure mass conservation, and $\xi(\mathbf{r},t)$ is the white noise which is directly related to the thermal fluctuation. Equation 4 is all we need to describe the evolution of crystal monolayers upon annealing. The time scales for the field are determined by the appropriate mobility D, and all other parameters correspond to their physical parts. The mass transport is not studied explicitly here because our interest is mainly on the nucleation stage, where the diffusion rate within the solid state only affects the magnitude but not the T-dependence of the nucleation rate. At later stage, the rate of growing the lateral size of thickening domains certainly can be controlled either by surface nucleation or by diffusion,[12] but it is beyond the main scope in this Communication.

Typical numerical results are shown in Figure 1e−h. Despite the time scale, a direct comparison between simulations and experiments can be made. In fact, the evolution patterns match each other remarkably well for many aspects, including (1) roughening (or fluctuation) of the top surface, (2) the present of induction period, (3) the curved shape of thickening domains, (4) the sigmoidal growth of H and linear growth of HW, and (5) the evolution of the number of thickening domains (see Supporting Information). This comparison confirms that the phase field simulation is versatile in reproducing the experimental observations.

In addition to these consistencies, the T-dependence of nucleation rate was also studied. Since the system in our simulation is rather small (256×256) bringing about the limited number of thickening domains, we determined the nucleation rate by running simulation with the same parameter set for a number of times and recording the appearing time of the first thickening domain which could survive to grow further for each run.[23] At long times the histogram $h(t)$ of these first appearing times behaves as $h(t) \sim \exp(-I_s t)$, where I_s denotes the nucleation rate obtained by simulation (see Supporting Information).

In simulation we found that the nucleation rate was quite sensitive to the property of σ_e. Keeping σ_e a constant would give the nucleation rate dropping with increasing T, contrary to the experimental observations. In light of the work of Flory and Vrij,[24] Kovacs and Buckley,[25] and Hoffman et al.,[21] we assume that σ_e of the amorphous fold surface can be expressed as $C - BT$, a linear decrease with T. Although no experimental quantities were directly applied, the simulation with proper values of C and B could successfully recover the experimental observations (see Figure 3c); i.e., the logarithm of nucleation rate decreases linearly with $1/T$. According to the phase field theory,[26] the line tension γ in 2D case can be calculated from $\gamma = \int_{1/2}^{1} [2b_a f_{local}(\phi)]^{1/2} \, d\phi$. While f_{local} does not change much with T, the line tension is mainly dependent on the coefficient of gradient term b_σ. As T increases, σ_e will become smaller and so as b_σ and γ. Consequently, stems can protrude out of the top surface more easily, yielding a higher nucleation rate. In other words, the surface free energy is mapped to the line tension which hinders the nucleation of thickening domains in our 2D model. It has become clear: the chain sliding motion provides the manner of thickening whereas the surface free energy decides whether or not the sliding motion can actually lead to the nucleation. Furthermore, if we keep the T and other parameters constant to perform numerical simulation, the nucleation rate decreases with increasing b_σ and the nucleation process stops beyond some critical value. This may explain why some folded chain crystals cannot thicken or only thicken at T rather close to T_m.[8] The reason is that the surface energy of their fold surfaces exceeds a critical value corresponding to a particular set of parameters.

The simulations elaborated that thickening domains might appear and vanish back and forth for several times before one domain eventually reached the size large enough to grow further. A more detailed analysis exhibited that some nascent thickening domains could grow both in thickness and lateral size before they vanished. This picture is fully consistent with the classical nucleation theory. It tells the existence of a barrier associated with the size of critical nuclei. Therefore, our monolayer system studied gives a unique example of observing the nascent nuclei directly as colloidal systems did.[27]

The simplest way to estimate the work needed to form a thickening domain is to treat the thickening domain as a disk with a radius of R_A and a uniform thickness represented by an effective ϕ_A (see Supporting Information). Then, the work can be readily evaluated from the free energy functional[28]

$$W = F[\phi(\mathbf{r}, t)] - F[\phi_0(\mathbf{r}, t)] = \pi\left[f(\phi_A) - 2\phi_A f\left(\frac{1}{2}\right)\right]R_A^2 + \pi b_\sigma \left(\phi_A - \frac{1}{2}\right)^2 R_A, \qquad (5)$$

The results of the numerical simulation are plotted in Figure 4 for different Ts, wherein the $W-R_A$ curve can be fitted satisfactorily with a quadratic function. The nucleation barrier W^* extracted from the fitted functions is linearly proportional to $1/T$ (see the inset). Therefore, the nucleation rate which can be calculated as $A \exp(-W^*) \propto \exp(-1/T)$ is consistent with both the simulation and experiment. We note that the R_A^* values corresponding to the W^* ranged from 2 to 4 are too small in comparison with experimental results, reflecting that in the phase field model a lattice point may be composed of several stems rather than one as assumed previously. However, the diameter of "stem" introduced in this model should be proportional to that of the real system, although we do not know the quantitative relationship between them.

In summary, we traced the thickening from IF(1) to IF(0) of the LMW PEO monolayer crystals on the mica surface using the in situ AFM method. The experiments have revealed the

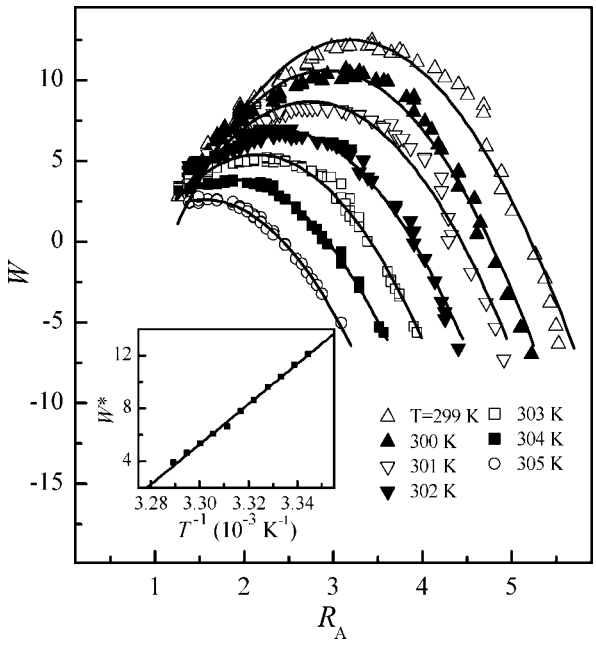

Figure 4. (a) Works needed to form a thickening domain calculated from simulation as functions of the thickening domain size at different *T*s. Solid lines are fitting curves of quadratic functions. (b) Nucleation barrier W^* (peak value of the fitted $W-R_A$ curve) as a linear function of T^{-1}.

detailed process of the morphological evolution via generating thickening domains in the mother phase. This transition follows a NG mechanism, which can be suitably tackled with the phase field simulation. The numerical study indicates that the increase in the thickening nucleation rate with T is mainly caused by the reduction of surface energy. Therefore, for metastable lamellar crystals of polymers, we may conclude that the tendency of reducing the free energy makes the thickening possible, the sliding motion of stems provides a means to overcome the barrier, and the fold surface properties govern the T-dependent behavior. We hope that this work would deepen our understanding of the polymer metastability and be extended to other complex reorganization and recrystallization behaviors of polymeric materials. Although in the present work we deal with the LMW PEO monolayers on solid substrates, the preliminary results may help to the further study of general mechanism of lamellar thickening. For high molecular weight (HMW) crystalline polymers, the excess energy due to the chain ends becomes negligible. Therefore, the lamellae can stay at the local energy minima of either integral or nonintegral folded states, depending on both time and temperatures. In this context, our LMW PEO, which always selects the two most profound free energy minima of IF(1) and IF(0), looks different. However, the local free energy (f_{local}) of LMW PEO in fact possesses many other local minima of fractionally folded crystals (see Supporting Information), which is thus essentially the same as that of HMW ones. The thickening from IF(1) to IF(0) shall not be a simple two-state system but rather a multiple-step process. After the barrier of IF(1) thickening is overcome, the following transient steps are hard to be monitored clearly due to the rapid kinetics with shallow barriers. At present, to completely explore the molecular details for the pathway of free energy changes during the thickening is a challenge task. As long as this complete free energy pathway is understood, the linkage between low and high molecular weight polymer crystals may be established.

Acknowledgment. The authors acknowledge the helpful comments from Dr. An-Chang Shi and Dr. Stephen Z. D. Cheng to this study. The financial support was provided by the National Nature Science Foundation of China (20234020, 20774006, and 20874019) and National Basic Research Program of China (2005CB623800).

Supporting Information Available: A sequence of AFM images of a monolayer crystal annealed at 30 °C; deconvolution of AFM section profiles; detailed calculation of eq 4 and its related parameters; simulation details; methods to calculate nucleation rate and nucleation barrier from simulation data. This material is available free of charge via the Internet at http://pubs.acs.org.

References and Notes

(1) Cheng, S. Z. D. *Phase Transitions in Polymers: The Role of Metastable States*; Elsevier: Amsterdam, 2008.
(2) (a) Mandelkern, L.; Posner, A. S.; Diorio, A. F.; Roberts, D. E. *J. Appl. Phys.* **1961**, *32*, 1509. (b) Fischer, E. W. *Angew. Chem., Int. Ed.* **1962**, *1*, 488.
(3) (a) Schultz, J. M. *J. Macromol. Sci., Part B: Phys.* **1970**, *4*, 775. (b) Schmidt-Rohr, K.; Spiess, H. W. *Macromolecules* **1991**, *24*, 5288. (c) Hirschinger, J.; Schaefer, D.; Spiess, H. W.; Lovinger, A. J. *Macromolecules* **1991**, *24*, 2428. (d) Hikosaka, M.; Amano, K.; Rastogi, S.; Keller, A. *Macromolecules* **1997**, *30*, 2067.
(4) (a) Sanchez, I. C.; Colson, J. P.; Eby, R. K. *J. Appl. Phys.* **1973**, *44*, 4332. (b) Sanchez, I. C.; Peterlin, A.; Eby, R. K.; McCrackin, F. L. *J. Appl. Phys.* **1974**, *45*, 4216.
(5) Peterlin, A. *J. Polym. Sci., Part B: Polym. Lett.* **1963**, *1*, 279.
(6) Kovacs, A. J.; Gonthier, A. *Colloid Polym. Sci.* **1972**, *250*, 530.
(7) Ichida, T.; Tsuji, M.; Murakami, S.; Kawaguchi, A.; Katayama, K. *Colloid Polym. Sci.* **1985**, *263*, 293.
(8) Wunderlich, B. *Macromolecular Physics*; Academic Press: New York, 1976; Vol. *2*.
(9) Reiter, G.; Sommer, J. U. *Polymer Crystallization: Observations, Concepts and Interpretations*; Springer-Verlag: Berlin, 2003.
(10) Schultz, J. M.; Miles, M. J. *J. Polym. Sci., Part B: Polym. Phys.* **1998**, *36*, 2311.
(11) Lei, Y. G.; Chan, C. M.; Li, J. X.; Ng, K. M.; Wang, Y.; Jiang, Y.; Li, L. *Macromolecules* **2002**, *35*, 6751.
(12) Zhu, D. S.; Liu, Y. X.; Chen, E. Q.; Li, M.; Chen, C.; Sun, Y. H.; Shi, A. C.; VanHorn, R. M.; Cheng, S. Z. D. *Macromolecules* **2007**, *40*, 1570.
(13) Sanz, N.; Hobbs, J. K.; Miles, M. J. *Langmuir* **2004**, *20*, 5989.
(14) Reiter, G.; Castelein, G.; Sommer, J. U. *Phys. Rev. Lett.* **2001**, *86*, 5918.
(15) Zhai, X.; Zhang, G.; Ma, Z.; Tang, X.; Wang, W. *Macromol. Chem. Phys.* **2007**, *208*, 651.
(16) (a) Cheng, S. Z. D.; Zhang, A.; Barley, J. S.; Chen, J.; Habenschuss, A.; Zschack, P. R. *Macromolecules* **1991**, *24*, 3937. (b) Cheng, S. Z. D. *J. Polym. Sci., Part B: Polym. Phys.* **1991**, *29*, 311.
(17) Takahashi, Y.; Tadokoro, H. *Macromolecules* **1973**, *6*, 672.
(18) Villarrubia, J. S. *J. Res. Natl. Inst. Stand. Technol.* **1997**, *102*, 425.
(19) (a) Chen, L. Q. *Annu. Rev. Mater. Res.* **2002**, *32*, 113. (b) Gránásy, L.; Pusztai, T.; Börzsönyi, T.; Tóth, G.; Tegze, G.; Warren, J. A.; Douglas, J. F., *J. Mater. Res.* **2006**, *21*, 309.
(20) Bray, A. J. *Adv. Phys.* **2002**, *51*, 481.
(21) Hoffman, J. D.; Davis, G. T.; Lauritzen, J. I. *Crystalline and Noncrystalline Solids*; Plenum Press: New York, 1976.
(22) Zachmann, H. G.; Peterlin, A. *J. Macromol. Sci., Part B: Phys.* **1969**, *3*, 495.
(23) (a) Brendel, K.; Barkema, G. T.; Beijeren, H. *Phys. Rev. E* **2005**, *71*, 31601. (b) Alford, M.; Feldman, H.; Gleiser, M. *Phys. Rev. D* **1993**, *47*, 2168.
(24) Flory, P. J.; Vrij, A. *J. Am. Chem. Soc.* **1963**, *85*, 3548.
(25) Buckley, C. P.; Kovacs, A. J. *Colloid Polym. Sci.* **1976**, *254*, 695.
(26) (a) Cahn, J. W.; Hilliard, J. E. *J. Chem. Phys.* **1958**, *28*, 258. (b) Elder, K. R.; Grant, M.; Provatas, N.; Kosterlitz, J. M. *Phys. Rev. E* **2001**, *64*, 21604.
(27) Zhang, T. H.; Liu, X. Y. *J. Am. Chem. Soc.* **2007**, *129*, 13520.
(28) Castro, M. *Phys. Rev. B* **2003**, *67*, 35412.

MA802806Q